PHYSICAL REVIEW B **90**, 184501 (2014)

Magnetic fields above the superconducting ferromagnet UCoGe

D. J. Hykel,[1,2] C. Paulsen,[1,2] D. Aoki,[3] J. R. Kirtley,[1,2,4] and K. Hasselbach[1,2]

[1]*Centre National de la Recherche Scientifique, Institut NEEL, F-38042 Grenoble Cedex 9, France*

[2]*Université Grenoble-Alpes, Institut NEEL, F-38042 Grenoble Cedex 9, France*

[3]*INAC/SPSMS, CEA-Grenoble, 17 rue des Martyrs, 38054 Grenoble, France*

[4]*Center for Probing the Nanoscale, Stanford University, Stanford, California 94304, USA*

(Received 29 April 2014; revised manuscript received 14 October 2014; published 4 November 2014)

We study how coexisting states of superconductivity and magnetism interact with each other by local measurements of the magnetic fields, with micron scale spatial resolution, above a single crystal of the ferromagnetic superconductor UCoGe using scanning superconducting quantum interference device microscopy. Our measurements show that the spontaneous ferromagnetic transition at $T_C = 2.5$ K is characterized by Ising-like magnetization along the easy axis (c direction), with domain sizes of the order of 10 μm, magnetization amplitudes of 45 G, and are consistent with estimates of domain-wall widths of several angstroms. The measured magnetization amplitudes are in agreement with bulk magnetization measurements, implying that domain reconstruction at the sample surface is negligible. In the superconducting state, which coexists with ferromagnetism below $T_{SC} = 0.67$ K, both diamagnetic screening and Meissner expulsion of flux, but no shrinkage of the ferromagnetic domains, are detected. Although we could not resolve individual vortices, our measurements provide evidence for the existence of the spontaneous vortex state in UCoGe.

DOI: 10.1103/PhysRevB.90.184501 PACS number(s): 74.25.Ha, 74.25.Op, 74.70.Tx, 74.70.Dd

I. INTRODUCTION

Superconductivity and magnetism have long been considered to be mutually exclusive quantum states of matter. Notably, long-range ferromagnetic order tends to break Cooper pairs formed by electrons of antialigned spins, although long-range antiferromagnetic order is compatible with superconductivity, as is short-range-order ferromagnetism, as long as the period of modulation is shorter then the superconducting coherence length. Such a coexistence of ferromagnetism (FM) and superconductivity (SC), called cryptoferromagnetism [1], was first observed in rare-earth compounds whose local moments order magnetically at temperatures inside a superconducting phase, and has been exemplified in $ErRh_4B_4$. The superconducting properties of these systems are governed by the $4d$ Rh electrons, while the $4f$ Er electrons act as localized moments [2]. In $ErRh_4B_4$, on lowering the temperature, ferromagnetic domains form and grow in size as the localized moments at the Er sites increase and superconductivity is destroyed [3]. The energy gain for ferromagnetic ordering is in general much larger than the gain in condensation energy of a superconductor, making coexistence of superconductivity and ferromagnetism only possible as long as the magnetic moment is small enough. The magnetic properties of these ferromagnetic superconductors are presented in a comprehensive review [4].

Recently a family of uranium based compounds with SC/FM coexistence has been discovered: UGe_2 [5], URhGe [6], and UIr_5 [7]. In this family the magnetism is itinerant and mediated by the extended $5f$ orbitals of the uranium atoms, which contribute also to the density of states at the Fermi level, as opposed to the localized magnetism in the chevrel and rare-earth tetraborides, and thus the same electrons may contribute to both quantum phenomena.

Since the discovery of the latest superconducting ferromagnet of this family, UCoGe [8,9], crystallizing in the orthorhombic TiNiSi structure (space group P_{nma}) just as URhGe, many bulk measurements have clearly shown the local coexistence of superconductivity and itinerant ferromagnetism [10–12]. Moreover, this coexistence is cooperative, at odds with standard BCS theory. Equal spin pairing, as indicated by the high upper critical fields, exceeding the Pauli limit [8,13,14], could be provided by spin fluctuations [15]. Bulk measurements also show that UCoGe is a perfect Ising magnet with a magnetization along the c axis and with a small ordered moment of up to $0.07\mu_B$. There is indirect evidence for this spontaneous vortex state in UCoGe [12,16]. Within this family of compounds only UCoGe and URhGe show SC/FM coexistence at ambient pressure. The superconducting transition temperature $T_{SC} \sim 0.5$ K and the Curie temperature $T_{Curie} \sim 2.5$ K of UCoGe make it a perfect candidate for scanning superconducting quantum interference device (SQUID) microscopy. In this work we provide evidence for the existence of the spontaneous vortex state from direct magnetic imaging, but conclude that the vortex density is too high to resolve individual vortices even at zero applied field. It has also been predicted that the onset of superconductivity will cause a dramatic shrinkage of the ferromagnetic domains [17]. We do not observe such a shrinkage.

II. EXPERIMENTAL METHODS

Our measurements were made with a high-resolution scanning SQUID microscope (SSM) working in a dilution refrigerator [18,19]. The microscope combines tuning fork based scanning force microscopy and magnetic microscopy using a μ-SQUID scanning parallel to the sample surface. The microscope is equipped with three piezoelectric motors for the coarse approach in the x, y, and z directions. A large range scanner moves the sample as much as 85 μm in the x and y directions relative to the μ-SQUID tip. By means of the novel upside down dilution refrigerator the sample can be cooled down to temperatures as low as 0.2 K. The square shaped aluminum μ-SQUID has an effective area of 1.21 μm^2, with

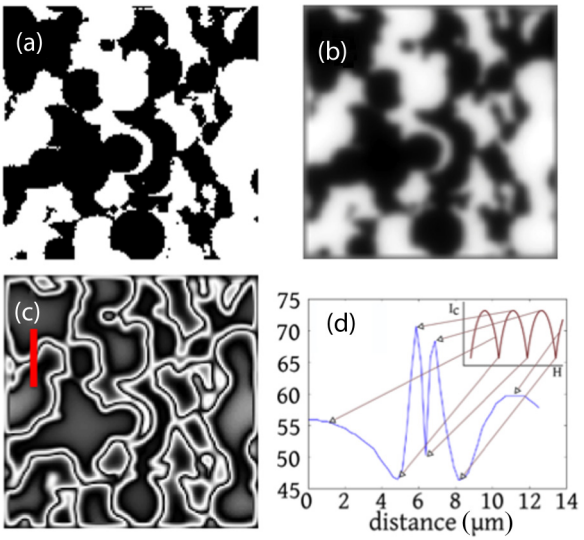

FIG. 1. (Color online) Interpretation of the critical current images: (a) Simulated magnetic field above a perfect Ising magnet with a complicated domain structure. (b) Image of the magnetic flux through the SQUID of 1.2 μm^2 area at a height of 400 nm above the surface. (c) Resulting critical current map. (d) Critical current profile along the line. The critical current crosses several minima and maxima. The start and end values are similar even though the end points are above domains with opposite signs of the magnetization.

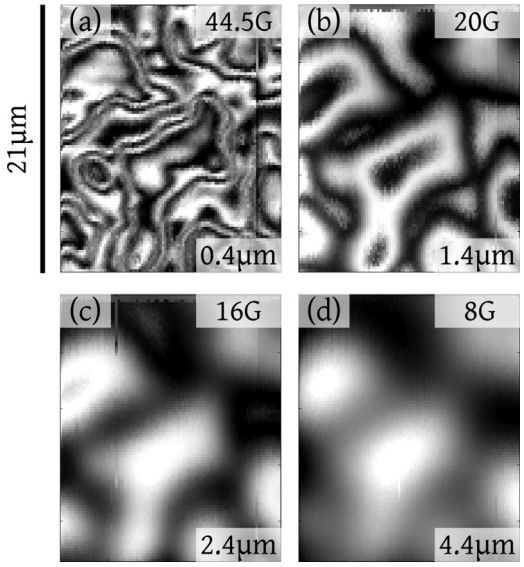

FIG. 2. Critical current maps taken at different sample surface - μ-SQUID spacings (heights) while scanning above the ab face of UCoGe at a temperature $T = 0.25$ K, well below the ferromagnetic (T_C) and superconducting (T_{SC}) transition temperatures. The sample was cooled in zero magnetic field, and no external field was applied. The heights and the magnetic contrast for each image are indicated.

Dayem bridges for weak links. These devices are hysteretic, so that they cannot be used in a flux-locked loop. Instead the current through the μ-SQUID is ramped until the transition into the voltage state at the critical current (I_c) is detected and recorded. The critical current of the μ-SQUID is a periodic function of the flux penetrating the SQUID loop, with period the superconducting flux quantum $\Phi_0 = hc/2e$. By repeatedly measuring the critical current we achieve a flux resolution of $1.2 \times 10^{-4}\Phi_0/\sqrt{\text{Hz}}$.

The images shown in this paper are maps of the critical current as a function of the SQUID's position above the surface. The magnetic fields near the surface of UCoGe have sufficient amplitude and change sufficiently rapidly that multiple branches of the I_c vs Φ curve are spanned in a single image. As the critical current is a periodic function of the flux penetrating the SQUID it may have accidentally the same value above domains of opposite magnetization, as illustrated in the simulation of Fig. 1. The line in Fig. 1 following the critical current profile crosses several arches from one domain center to the next. However, the assignment of various sections of the images to different arches can be made by making critical current maps above the same sample position at different sample-μ-SQUID spacings (Fig. 2). The sharply defined double fringes in Fig. 2(a) can be identified as domain boundaries with the help of Figs. 2(c) and 2(d).

Our SSM images are consistent with UCoGe having a domain structure of a perfect Ising magnet, with magnetization either parallel or antiparallel to the easy (c) axis. In UCoGe the anisotropy energy K is dominant compared to the exchange energy ($\propto T_{\text{Curie}} = 2.5$ K): applied fields as high as $\mu_0 H = 55$ T are not sufficient to turn the hard axis magnetization (a) along the easy axis [20]. Thus it is only possible to give a lower limit for the anisotropy constant K of at least 3×10^5 J/m^3. To estimate the order of magnitude of the domain-wall width [21], $\delta = \sqrt{\frac{JS^2\pi^2}{Ka}}$, $J = nk_B T_C$, $n = 0.15$ with $S = 0.02$, lattice constant $a \sim 6$ Å, $T_{FM} = 2.5$ K, and the lower bound of the anisotropy constant of UCoGe $K = 3 \times 10^5$ J/m^3, yields an upper limit for the domain-wall thickness of $\delta \sim 0.1$ Å, comforting us in the Ising-like nature of the domain walls present in UCoGe.

III. EXPERIMENTAL RESULTS

The sample was a UCoGe single crystal with dimensions of 340 μm along the c direction, 290 μm (b), and 1.11 mm (a), and 1.2 mg weight. The sample preparation is discussed elsewhere [22]. The sample has been characterized by resistivity and specific-heat measurements using a physical property measurement system (PPMS) ^{3}He system. Magnetization and susceptibility have been measured in the low-temperature (0.07 K) SQUID setup developed at the Néel Institute. This setup is equipped with a μ metal shield and a superconducting shield with a residual field of less than 5 mG. The absolute values of magnetization and susceptibility were obtained by the extraction method.

The results of the various bulk measurements used to characterize the sample are displayed in Fig. 3. Figure 3(a) shows the low-temperature part of the resistivity of the sample with the current applied along the a axis of the single crystal. An anomaly in the resistivity is clearly visible at $T_C \sim 2.45$ K which corresponds to the ferromagnetic transition. Well below this temperature, the onset of the superconducting transition appears at $\simeq 0.67$ K and is complete at 0.45 K. The specific-heat measurement, Fig. 3(b), shows the ferromagnetic

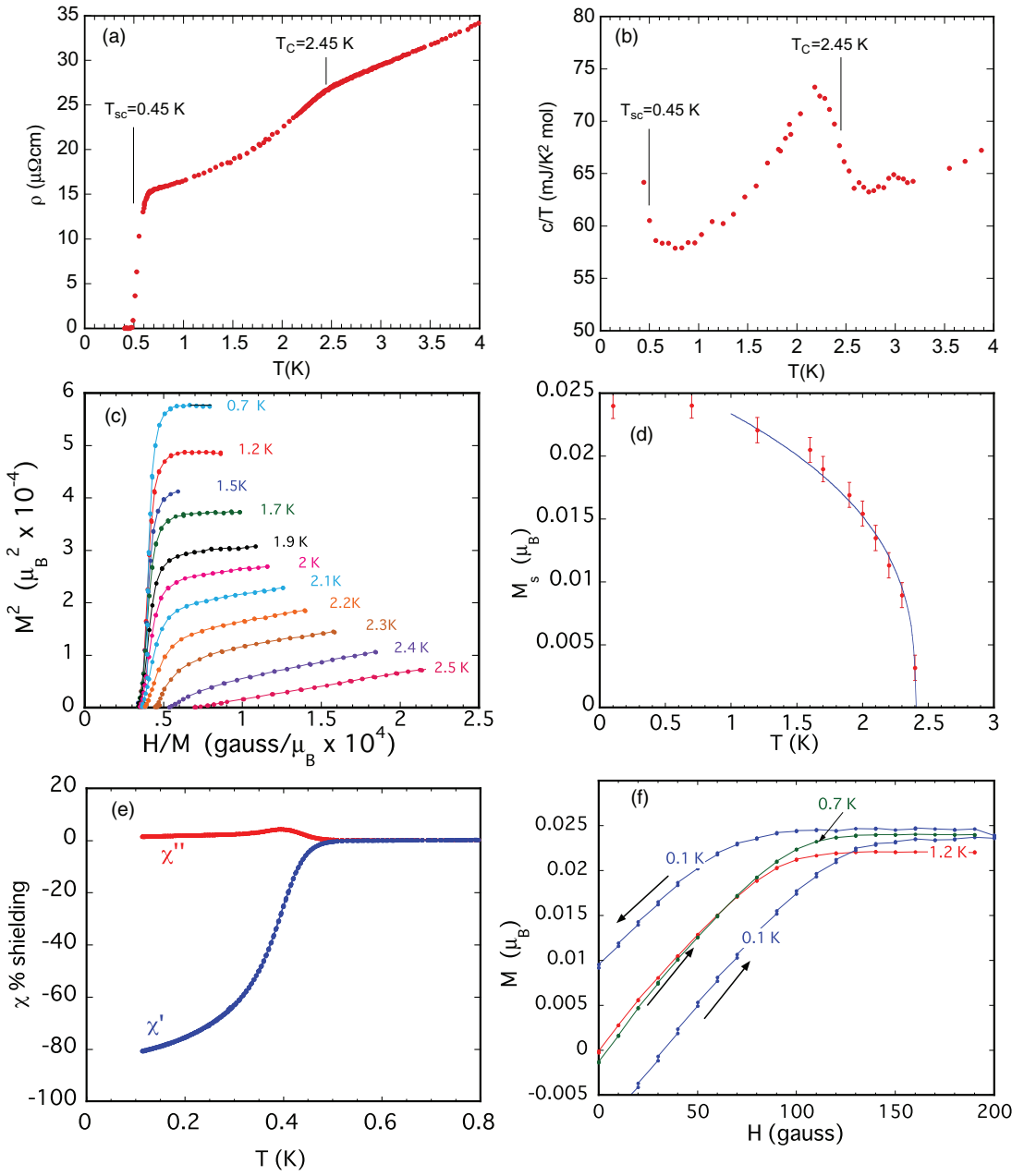

FIG. 3. (Color online) (a) The resistivity of the UCoGe sample shows an anomaly at the ferromagnetic transition $T_C = 2.45$ K, and the transition to the superconducting state is complete at $T_{SC} = 0.45$ K. The residual resistance ratio is approximately 19. (b) Specific heat as a function of temperature. The ferromagnetic transition appears at the onset of a significant peak at $T_C = 2.45$ K, the height of which is of the same order as the anomaly seen for the beginning of the superconducting transition at $T_{SC} = 0.45$ K. (c) Arrott plot of magnetization squared vs H/M. (d) The spontaneous moment inferred from the Arrott plot vs T. (e) The real and imaginary parts of the low-field ac susceptibility measured at 5.7 Hz and in a field of 0.25 Oe_{rms}. The onset of superconductivity by ac susceptibility is at approximately 0.5 K and at low temperature 80% screening occurs. (f) Hysteresis plots of magnetization M vs applied field H along the c axis for selected temperatures.

transition at $T_C \sim 2.45$ K and the onset of the superconducting transition at $T_{SC} \simeq 0.45$ K.

Figure 3(c) shows magnetization curves made at various fixed temperatures displayed in an Arrott plot as M^2 vs H/M. The field direction was along the easy (c) axis. From this plot it can be seen that the ferromagnetic transition occurs around 2.4 K, but it is somewhat smeared out over approximately 30 mK. The spontaneous moment M_S deduced from the Arrott plot is shown vs temperature in Fig. 3(d). The blue line is a scaling fit $M_S \sim (1 - T/T_C)^\beta$ over the temperature range 1–2.5 K, and gives a critical exponent $\beta \simeq 0.34$ and $T_C \simeq 2.4$. The spontaneous magnetization at 700 mK, above the superconducting transition is $M_S = 0.024\mu_B$. This value is significantly smaller than the effective moment $\sim 1.5\mu_B$ deduced from the Curie constant at high temperature in the paramagnetic phase but is consistent with weak ferromagnetism.

The real and imaginary parts of the ac susceptibility with the field applied along the c axis are shown in Fig. 3(e). The

frequency for these measurements was 5.7 Hz and the applied field was 0.25 Oe rms. The data have been corrected for demagnetization effects and plotted as the percent shielding (i.e., perfect shielding -100% corresponds to $\chi = -1/4\pi$, or -1 in SI units). The onset of magnetic shielding begins is at $\sim$0.5 K. At low temperatures the shielding is large, attaining about 80% perfect shielding, but never complete even within the errors of the demagnetization corrections. (The demagnetization factor was estimated to be 5 ± 0.5 in cgs units along this direction.)

The hysteresis measured along the c axis at 100 mK in the superconducting state is shown in Fig. 3(f), as well as two increasing field branches of the magnetization measured at 1.2 K and 700 mK. The hysteresis in the ferromagnetic state above the superconducting transition is small, the coercive field is approximately 6 G for this sample at 700 mK, which implies relatively weak pinning of domain walls. Below the superconducting transition, the coercive field increases more rapidly, reaching a value of approximately 32 G at 100 mK. Note that the increasing field branch of the hysteresis at 100 mK is actually less than that measured at 700 mK, above the superconducting transition. This is caused by the diamagnetic shielding for increasing fields in the superconducting state.

We present magnetic imaging measurements done above the ab plane of this sample, parallel to the magnetic easy axis c, as we expect to see in this geometry the most significant features of the interplay between superconductivity and ferromagnetism.

A. Ferromagnetic transition

When zero-field cooling (ZFC) the sample from 2.8 K to 250 mK, we observe the spontaneous creation of domain structures as shown in Figs. 4(a)–4(d). This demonstrates that ferromagnetic order over a scale of tens of microns is present, at variance with [23], which reports no long-range ferromagnetic order in zero field. The domain structure is complex, with instances of domains of the same sign isolated from each other and embedded in a larger domain of the opposite sign.

In Fig. 4(a) a magnetic contrast of 2.4 G between the maximum and minimum field values develops, indicating that precursors of magnetic order appear at temperatures as high as 2.8 K. As the temperature decreases, the magnetic contrast becomes larger, and domain walls become apparent. By counting the critical current periods crossed from the center of one domain to the next [as indicated by the line in Fig. 4(d)] it is possible to determine that there is a magnetic field $B_{\rm ext} \approx \pm 22$ G above the domains (i.e., 1/2 the magnetic contrast). If we assume a domain geometry of a long tube of diameter $d = 10$ μm and length $l = 340$ μm that spans the height of the sample from top to bottom, then the field inside the middle of the domain would be twice the value at the ends, $B_{\rm in} = 45$ G (as in a long solenoid). This is in good agreement with bulk measurements of the spontaneous magnetization, which give $B_{\rm bulk} = 4\pi M = 52$ G for this sample. The fact that the magnetic field above a domain corresponds to bulk magnetization measurements indicates that domain reconstruction close to the sample surface is very weak, and is consistent with our estimate of a very large anisotropy and narrow domain walls. Repeating the ZFC procedure from above 2.8 K results in different domain structures, indicating weak nucleation centers and domain-wall trapping.

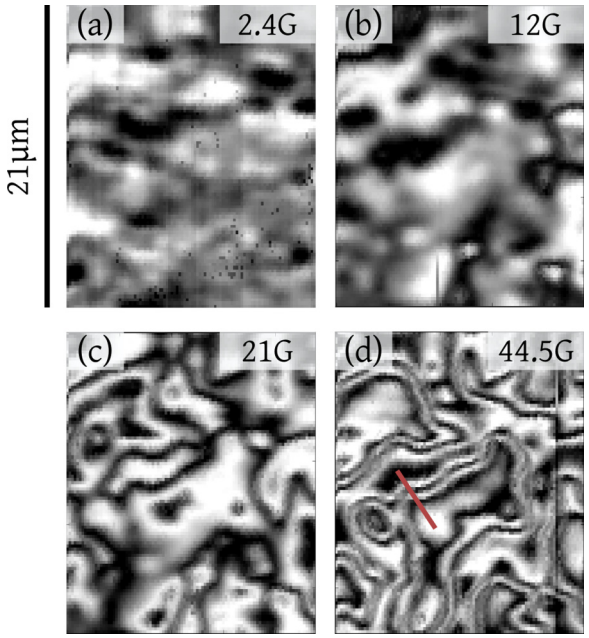

FIG. 4. (Color online) Ferromagnetic transition (ZFC, imaging ab plane): (a) A precursor of magnetic ordering can already be observed at 2.8 K. (b) At 1.8 K larger magnetic structures become visible. (c) At $T = 0.6$ K, just above $T_{\rm SC}$, the magnetic signal has become larger than the period of the SQUID characteristic of 16.8 G, leading to a nonmonotonic map. (d) The domain structure in the superconducting state at 250 mK. No change in the domain structure could be observed between 0.6 K and 250 mK. The largest domain has a size of about 20 μm. The field difference above two opposite domains can be deduced by analyzing the critical current profile along the line.

B. Superconducting screening and Meissner expulsion

For conventional superconductors, local scanning SQUID microscopy measurements are well suited to observe the diamagnetic screening from superconducting surface currents and the expulsion of flux due to the Meissner effect. A standard protocol for the experiments is to first zero-field cool the sample, then apply a field, then warm the sample above $T_{\rm SC}$, and finally recool in the same field, during which images of the sample are taken at each step. Thus for example, after ZFC and applying a field such that $H_{\rm app} < H_{c1}$, the bulk of the sample will be void of vortices. If on the other hand $H_{\rm app} > H_{c1}$ then vortices will penetrate the sample appearing at first along the edge, and penetrating to a depth such that the shielding current density is just equal to the critical current density according to the Bean model. After warming the sample and cooling in the applied field, vortices can be observed inside the sample. Their density depends on many factors: pinning sites, magnitude of the field, etc. However the net flux measured over the surface of the sample will be diminished because of the Meissner expulsion.

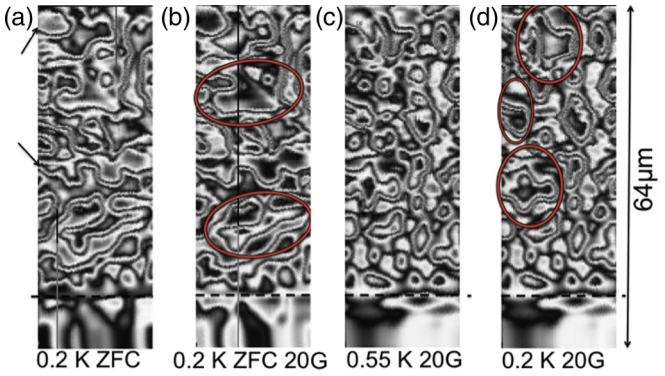

FIG. 5. (Color online) Magnetic imaging of the field- and temperature-dependent domain structure in UCoGe: (a) The sample is ZFC into the SC state. (b) An applied field of 20 G along the easy axis (c direction) shifts the color scale as the field over the entire image increases. The dashed line indicates the sample border, the top arrow points to a region where the magnetization in a domain changes, and the bottom arrow indicates a domain wall that has moved slightly: diamagnetic screening cannot be resolved. (c) Upon warming to 550 mK ($>T_{SC}$) some domains (as indicated by the circles) have broken up into several smaller ones. (d) Field cooling the sample leads to a local re-arrangement of the domain size near the sample edge. This could be due to flux expulsion from the region between 10 and 50 μm from the sample edge.

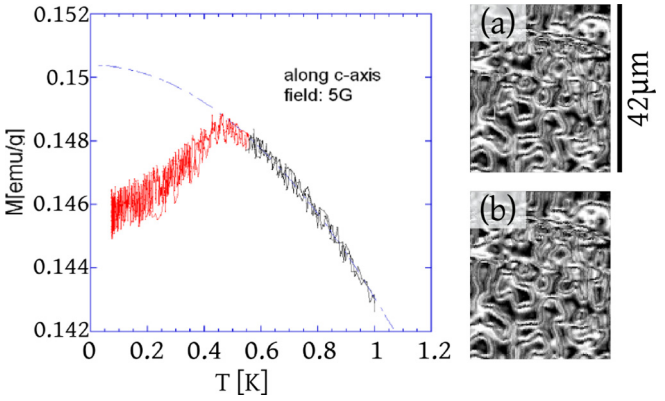

FIG. 6. (Color online) Magnetization measurements show an increasing magnetization with decreasing temperature. At the SC transition the magnetization drops as flux is expelled due to the Meissner effect. However, no change is observed above the center of the sample when field cooling (5 G): (a) at 550 mK, (b) 200 mK.

We have used the same protocol on the ferromagnetic superconductor UCoGe: The sample was first warmed in zero field above T_C to 3 K, and then cooled to below 200 mK and an image was taken. Then a field was applied, and the same region was imaged again. Each image takes about an hour for acquiring 80 × 240 pixels. Thus, Fig. 5(a) shows the sample after ZFC, and Fig. 5(b) after 20 Oe has been applied. Note that although we can cool in zero externally applied field, for UCoGe a field of approximately 52 G still exists inside the sample, arising from the spontaneous magnetic moment. Note also that we estimate H_{c1} along the c axis to be approximately 3 G [16].

Upon applying a 20-G field to a ZFC sample [compare Figs. 5(a) and 5(b)], the domain boundaries remain very similar, with only a few domain borders slightly displaced, e.g., the meandering line in the center. However, the magnetization changes in each domain: grey regions become white and white regions become grey, as magnetic field penetrates the sample over the entire image (see for example the round domain at the top left corner). Such a change in color corresponds to a change in magnetic induction of the order of 8 G. The overall shift in magnetization may be attributed to a homogenous penetration of vortices if the applied field is higher than H_{c1}, and thus the sample is not keeping all of the flux of the applied field of 20 G from penetrating. We will argue below that the high local induction produces vortices too close together to resolve with the SSM.

However, when the sample is subsequently warmed to 550 mK, above T_c, with unchanged applied magnetic field, we observe [see Fig. 5(c)] that the large circular domains split up to form many smaller domains, as if the disappearance of the vortices makes the large domains unstable.

In order to observe the Meissner effect at the edge of the sample, the sample was first warmed above T_c in 20 G, and then cooled in that field [see Fig. 5(d)]. Within 10 μm of the sample edge the domain configuration and the domain magnetization do not change. However, changes in the domain structure are visible between 10 and 50 μm from the sample edge: The circular domains seem to increase in size or to merge with neighboring domains upon field cooling. This seems consistent with the interpretation that applied flux is expelled from this region.

Theoretical calculations [17] suggest that the domain structure of a superconducting ferromagnet becomes smaller when transiting from the normal to the SC state. We did not observe a measurable change in the domain size at the sample center [compare Figs. 5(a) and 5(b)]. However, a difference in the average domain size can be observed when the following protocol is applied: First the sample was ZFC below T_{SC} (a) and then a magnetic field of 20 G was applied (b). Next, we warmed up the sample above T_{SC}, and we obtain a smaller domain structure in the normal phase. Cooling the sample back into the SC state results in some domains merging (not depicted), meaning that the domain structure is smaller in the normal state than in the superconducting state, in contrast to the theoretical prediction [17].

When crossing T_{SC} during cool-down bulk magnetization measurements show a weak decrease in magnetization due to Meissner expulsion (see Fig. 6, left panel) although the Meissner expulsion is too weak to be observed on the local scale at the sample center [Figs. 6(a) and 6(b)]. The size of the Meissner expulsion effect will be discussed below.

IV. DISCUSSION

A. Magnetic fields in a magnetic superconductor

In order to interpret the results above, we solve London's equation for the case of a magnetic superconductor in various scenarios. Consider a geometry in which the magnetic superconductor occupies the half-space $z < 0$, with $z > 0$ being free space. Following Bluhm [24], the magnetic induction $\mathbf{B}(\mathbf{r})$ in the superconductor is the solution of the inhomogeneous

London equation

$$\nabla \times \nabla \times \mathbf{B}(\mathbf{r}) + \mathbf{B}(\mathbf{r})/\lambda^2 = 4\pi \nabla \times \nabla \times \mathbf{M}(\mathbf{r}) + \frac{\Phi_0}{\lambda^2} \sum_i \delta(\mathbf{r}_{||} - \mathbf{r}_{\mathbf{i},||})\hat{z}, \quad (1)$$

where $\mathbf{M}(\mathbf{r})$ is the magnetization, $\Phi_0 = hc/2e$ is the superconducting flux quantum, the penetration depth λ is assumed to be independent of position inside the magnetic superconductor, and there are δ functions at the positions of the superconducting vortices $\mathbf{r}_{i,||}$, which are assumed to be oriented with their cores normal to the surface. For $z > 0$ $\mathbf{B} = -\nabla\Phi$, where the scalar potential Φ is the solution of $\nabla^2\Phi = 0$. The solution for $z < 0$ is given by

$$\mathbf{B} = \mathbf{B_0} + \mathbf{B_1}, \quad (2)$$

where $\mathbf{B}_0$ is a particular solution to the inhomogeneous London equation (1) over all space with appropriate boundary conditions at infinity, and $\mathbf{B}_1$ is a general solution of the homogeneous London equation [Eq. (1) with the right-hand side set equal to zero), chosen to satisfy the boundary conditions at $z = 0$. Expanding in Fourier series in the xy plane

$$\mathbf{A}(\mathbf{r}_{||},z) = \frac{1}{2\pi^2} \int d^2\mathbf{k}_{||} \tilde{\mathbf{A}}(\mathbf{k}_{||},z) e^{i(\mathbf{k}_{||}\cdot\mathbf{r}_{||})}, \quad (3)$$

where $\mathbf{A}$ represents, e.g., $\mathbf{B_0}$, $\mathbf{B_1}$, or $\mathbf{M}$, $\mathbf{r}_{||} = x\hat{x} + y\hat{y}$ and $\mathbf{k}_{||} = k_x\hat{x} + k_y\hat{y}$, leads to

$$(k^2 + 1/\lambda^2)\tilde{\mathbf{B}}_1 - \partial^2\tilde{\mathbf{B}}_1/\partial z^2 = 0, \quad (4)$$

where $k = |\mathbf{k}_{||}| = \sqrt{k_x^2 + k_y^2}$. Since $\tilde{\mathbf{B}}_\mathbf{1}$ must go to zero as $z \to -\infty$, we can write $\tilde{\mathbf{B}}_\mathbf{1} = \mathbf{B_K} e^{Kz}$, with $K = \sqrt{k^2 + 1/\lambda^2}$. Similarly for $z > 0$ we can write $\tilde{\Phi}(\mathbf{k}_{||},z) = \Phi_k(\mathbf{k}_{||})e^{-kz}$, which leads to

$$\tilde{\mathbf{B}}(\mathbf{k}_{||},z) = (-i\mathbf{k}_{||} + k\hat{z})\Phi_k(\mathbf{k}_{||})e^{-kz}. \quad (5)$$

The conditions $\nabla \cdot \mathbf{B} = 0$, as well as continuity of B_z and continuity of $\mathbf{k}_{||} \cdot \mathbf{H}$ at $z = 0$, where $\mathbf{H} = \mathbf{B} - 4\pi\mathbf{M}$, lead to the set of equations

$$\begin{aligned} 0 &= i\mathbf{k}_{||} \cdot \mathbf{B}_K + K\hat{z} \cdot \mathbf{B}_K, \\ k\Phi_k &= \hat{z} \cdot [\mathbf{B}_K + \tilde{\mathbf{B}}_0(\mathbf{k}_{||},0)] \\ -ik\Phi_k &= \hat{k}_{||} \cdot [\mathbf{B}_K + \tilde{\mathbf{B}}_0(\mathbf{k}_{||},0) - 4\pi\tilde{\mathbf{M}}(\mathbf{k}_{||},0)]. \end{aligned} \quad (6)$$

The components of the general solution parallel ($\hat{k}_{||} \cdot \mathbf{B_K}$) and perpendicular ($\hat{z} \cdot \mathbf{B_K}$) to the surface can be eliminated from Eqs. (6) to obtain a relation between the scalar potential outside the superconductor Φ_K, the inhomogeneous solution $\tilde{\mathbf{B}}_0$, and the magnetization $\tilde{\mathbf{M}}$:

$$k(k + K)\Phi_K = K\hat{z} \cdot \tilde{\mathbf{B}}_0(\mathbf{k}_{||},0) + i\mathbf{k}_{||} \cdot [\tilde{\mathbf{B}}_0(\mathbf{k}_{||},0) - 4\pi\tilde{\mathbf{M}}(\mathbf{k}_{||},0)]. \quad (7)$$

The inhomogeneous solution $\tilde{\mathbf{B}}_0$ is the solution of

$$-\mathbf{q} \times (\mathbf{q} \times \tilde{\mathbf{B}}_0) + \tilde{\mathbf{B}}_0/\lambda^2 = -4\pi\mathbf{q} \times (\mathbf{q} \times \tilde{\mathbf{M}}) + \sum_i \frac{\Phi_0}{\lambda^2} e^{-i\mathbf{k}_{||}\cdot\mathbf{r}_{||}}\hat{z}, \quad (8)$$

with $\mathbf{q} = \mathbf{k}_{||} + q_z\hat{z}$.

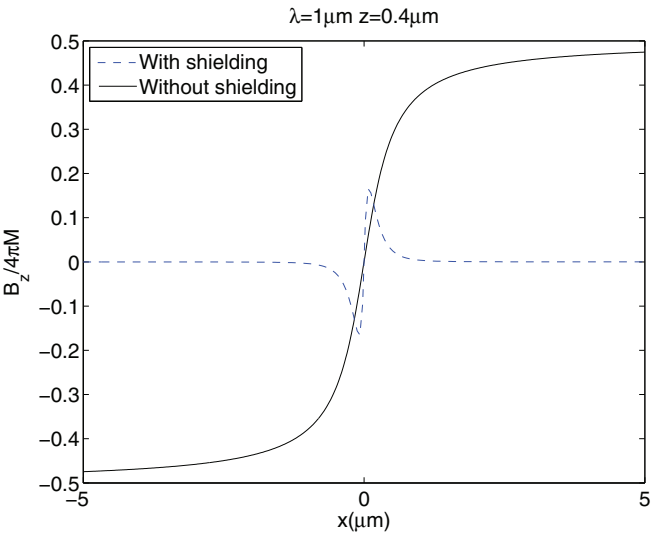

FIG. 7. (Color online) B_z, the component of the magnetic induction perpendicular to the surface, for a magnetic superconductor with penetration depth $\lambda = 1$ μm and magnetization $\mathbf{M} = M\text{sgn}(x)\hat{z}$, a height $z = 0.4\lambda$ above the surface. The solid line is the result Eq. (11) for no superconducting shielding; the dashed line is for superconducting shielding without forming vortices.

B. Meissner state

Consider first the situation in which the superconductor shields the magnetism without forming vortices. Tachiki [25] reports that this will happen if the magnetization satisfies $4\pi M < H_{c1}^0$, where H_{c1}^0 is the lower critical field for the superconductor in the absence of magnetism. For what follows, we neglect any z dependence of the magnetization $\mathbf{M}$ (aside from it being zero for $z > 0$), since the domains in UCoGe are apparently larger than the superconducting penetration depth. Then Eq. (8) becomes

$$(k^2 + 1/\lambda^2)\tilde{\mathbf{B}}_0 = 4\pi k^2\tilde{\mathbf{M}}. \quad (9)$$

For the case of a uniform magnetization perpendicular to the surface $\tilde{\mathbf{M}} = M\delta(\mathbf{k}_{||})\hat{z}$ the Fourier transform of the z component of the magnetic induction outside of the superconductor is given by

$$\tilde{B}_z = \frac{4\pi M K k^2 e^{-kz}\delta(\mathbf{k}_{||})}{(k + K)(k^2 + 1/\lambda^2)}. \quad (10)$$

This implies that there is *no* magnetic field above a magnetic superconductor with a single magnetic domain oriented perpendicular to the surface in the Meissner state, and $B_z = 2\pi M$ in the normal state. For a domain wall $\mathbf{M}(\mathbf{r}_{||},z) = M\text{sgn}(x)\hat{z}$ [24]

$$B_z = 4M \int_{-\infty}^{\infty} dk \frac{-ikK}{(|k| + K)(k^2 + 1/\lambda^2)} e^{ikx} e^{-|k|z}. \quad (11)$$

This is plotted as the dashed line in Fig. 7.

The z component of the magnetic field above a magnetic superconductor with magnetization $\mathbf{M} = M\text{sgn}(x)\hat{z}$ in the normal state is given by

$$B_z = -2iM \int_0^{\infty} dk\, e^{-kz}(e^{ikx} - e^{-ikx})/k. \quad (12)$$

This is plotted as the solid line in Fig. 7. Note that there is a huge difference between the normal and Meissner superconducting states in the magnetic field amplitudes and spatial distributions, for both uniform magnetization and for a domain boundary. The SQUID microscope measurements on UCoGe are inconsistent with it being in the Meissner state with no spontaneous vortices.

C. Spontaneous vortex state

If, as we believe, UCoGe enters the spontaneous vortex state, why don't our SQUID imaging experiments on UCoGe see vortices? The answer could be that the magnetization produces such large fields that the vortices are too close together to resolve. We assume for simplicity that the magnetization of the superconductor does not depend on the magnetic fields in the superconductor. Then we can solve for a single vortex located at $\mathbf{r}_{||} = 0$, and superpose solutions for a collection of vortices. If the magnetization $\mathbf{M}$ is spatially independent the Fourier transform of the z component of the field a height z above the surface is given by

$$\tilde{B}_z = \frac{\Phi_0 e^{-kz}}{\lambda^2 K(k+K)}. \tag{13}$$

The inverse Fourier transform gives

$$B_z(r,z) = \frac{\Phi_0}{2\pi\lambda^2}\int_0^\infty dk \frac{k e^{-kz} J_0(kr)}{K(k+K)}. \tag{14}$$

This is exactly the same as for a nonmagnetic superconductor [26].

The next question is: How dense do we expect the spontaneously generated vortices to be? Assume for the moment that vortex pinning is weak, and that the vortices form a triangular lattice. We then calculate the free energy as a function of the lattice constant a, and assume that the spontaneous vortex lattice has the density with the minimum energy. In the following we assume that the vortex cores are oriented in the z direction, parallel to the magnetization, neglect demagnetization effects, consider only the vortex fields deep within the superconductor, and neglect the vortex core energies. The electromagnetic energy component f of the free energy per unit volume of a vortex lattice is given by [27]

$$f = \frac{1}{8\pi}\{\mathbf{H}^2 + (\lambda\nabla\times\mathbf{H})^2\}. \tag{15}$$

Deep within the superconductor, the magnetic induction due to the vortex lattice is given by

$$\mathbf{B}(\mathbf{r}) = \sum_{n,m}\frac{\Phi_0}{2\pi\lambda^2}K_0(\beta)\hat{z}, \tag{16}$$

where K_ν is the modified Bessel function of the second kind of order ν, $\beta = |\mathbf{r}-\mathbf{r}_{\mathbf{n},\mathbf{m}}|/\lambda$ for $|\mathbf{r}-\mathbf{r}_{\mathbf{n},\mathbf{m}}| > \xi$, and $\beta = \xi/\lambda$ for $|\mathbf{r}-\mathbf{r}_{\mathbf{n},\mathbf{m}}| < \xi$, ξ is the superconducting coherence length, and the sum is over a triangular lattice in the xy plane $\mathbf{r}_{\mathbf{n},\mathbf{m}} = a(n\mathbf{r_1} + m\mathbf{r_2})$ with $\mathbf{r}_1 = [1,0]$ and $\mathbf{r}_2 = [\frac{1}{2}, \frac{\sqrt{3}}{2}]$, with n,m being integers. The average flux density is $\langle B_z\rangle = 2\Phi_0/\sqrt{3}a^2$. The solid symbols in Fig. 8 are a numerical evaluation of the area average of Eqs. (15) and (16) for $4\pi M = 45$ G, $\lambda = 1$ μm and $\xi = 12$ nm, using $\mathbf{H} = \mathbf{B} - 4\pi\mathbf{M}$ with $\mathbf{M} = M\hat{z}$.

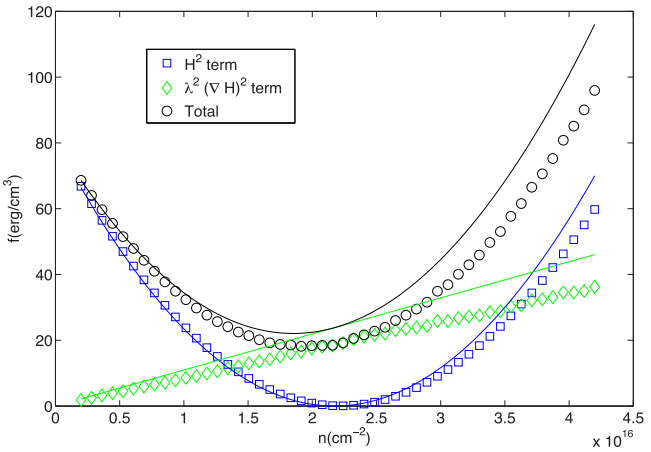

FIG. 8. (Color online) Plot of $\langle f\rangle$, the area average of the electromagnetic component of the free-energy density of a triangular vortex lattice as a function of the vortex density n, for a magnetic superconductor with a magnetization $4\pi M = 45$ G, $\lambda = 1$ μm, and $\xi = 12$ nm. The symbols are a numerical evaluation of Eqs. (15) and (16). The solid lines are the analytical approximations, Eqs. (17) and (18).

At the relevant values for the magnetization and penetration depth the vortex fields do not depend strongly on position, and the term proportional to $\mathbf{H}^2$ in Eq. (15) can be approximated by

$$\langle f_{1,a}\rangle = \frac{\Phi_0^2}{8\pi}(n-n_0)^2, \tag{17}$$

where n is the vortex density and $n_0 \equiv 4\pi M/\Phi_0$. The term proportional to $(\nabla\times\mathbf{H})^2$ in Eq. (15) is dominated by the strong gradients close to the vortex cores. Using $\nabla\times\mathbf{H} = dH_z/dr\hat{\phi}$, $dK_0(x)/dx = -K_1(x)$, and $\int_\xi^\infty x(K_1(x))^2 = \frac{\xi^2}{2}[K_0(\xi)K_2(\xi) - (K_1(\xi))^2]$, this term can be approximated as

$$\langle f_{2,a}\rangle = \frac{\Phi_0^2\xi^2 n}{32\pi^2\lambda^2}\left[K_0(\xi/\lambda)K_2(\xi/\lambda) - K_1^2(\xi/\lambda)\right]. \tag{18}$$

The approximations $\langle f_{1,a}\rangle$, $\langle f_{2,a}\rangle$ and their sum are plotted as the solid lines in Fig. 8. The vortex lattice is calculated to have a minimum energy at a magnetic flux density which is about 15% lower than the normal-state magnetization using the analytical approximations with $\lambda = 1$ μm [28] and $\xi = 12$ nm. The numerical results are about 11% lower. We would therefore expect the Meissner flux expulsion to be approximately 11–15% of the magnetization of the sample for a single domain. The experimental result is about 3%.

It is therefore a good first guess that the spontaneous vortex density $n \sim 4\pi M/\Phi_0$. Figure 9 shows the magnetic field a height $z = 0.4\lambda$ above the surface for various values of the lattice spacing a, assuming a perfect triangular lattice. The average field above a particular domain in UGeCo in the SQUID microscopy experiments is approximately 25 G. This corresponds to $a \sim 1$ μm, or $a/\lambda \sim 1$. Figure 9(a) shows that at this density, height ($z = 0.4$ μm), and penetration depth the vortices strongly overlap and there is little contrast in the magnetic field image.

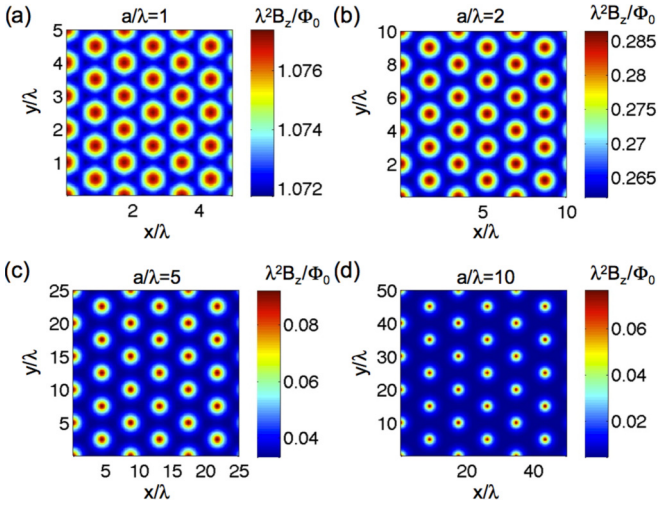

FIG. 9. (Color online) Normalized B_z a height $z = 0.4\lambda$ above the surface for the spontaneous vortex state, assuming a triangular lattice for the vortex positions, with vortex spacings a/λ as labeled in the figure.

Figure 10 displays the calculated flux image for a square SQUID with side $s = \lambda$, at a height $z = 0.4\lambda$, for the same lattice spacings as in Fig. 9. For $a \sim \lambda$ the vortex images overlap significantly, sharply reducing the contrast in the images. The "stripes" in Fig. 10(a) are due to the fact that we are scanning a square SQUID relative to a triangular lattice.

Figure 11 plots $\Delta\Phi_s/\Phi_0$, the difference between the maximum and the minimum values of the flux images, as a function of a/λ for selected values of the SQUID size s/λ, at a height $z/\lambda = 0.4$. The magnetic contrast falls off exponentially when the vortex spacing becomes comparable to either the

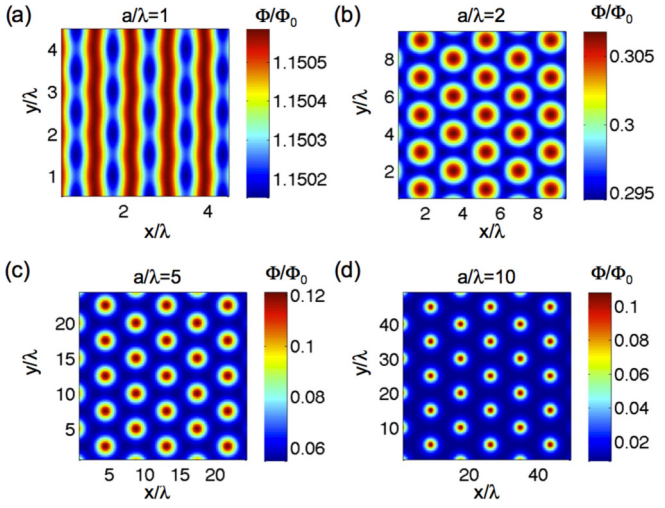

FIG. 10. (Color online) Magnetic flux through a square area of side $s = \lambda$, a height $z = 0.4\lambda$ above the surface for the spontaneous vortex state, assuming a triangular lattice for the vortex positions, with vortex densities a/λ as labeled in the figure. The "stripes" in (a) result from the relative alignment of the square area, assumed to have sides parallel to the x and y directions, and the unit-cell axes of the triangular lattice.

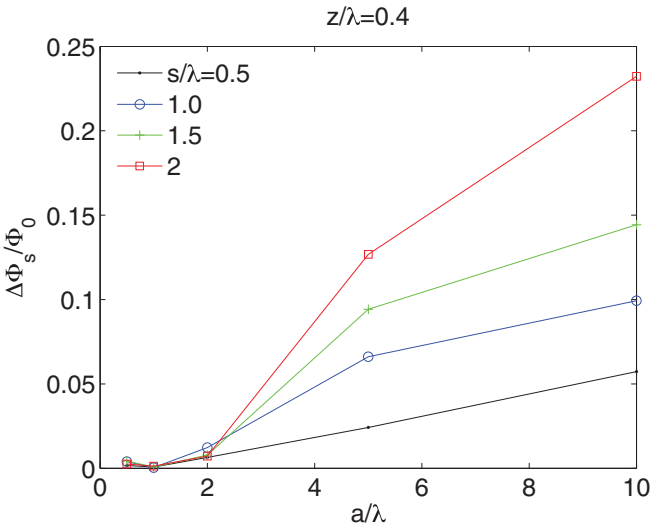

FIG. 11. (Color online) Variation $\Delta\Phi$ between the maximum and minimum of the flux through a square area with side s a height $z = 0.4\lambda$ above the surface for the spontaneous vortex state, assuming a triangular lattice for the vortex positions, as a function of the vortex lattice spacing a, for various values of s/λ.

penetration depth or the SQUID size, as expected for UCoGe and our SQUID size of 1.1 μm. Thus, the fact that we do not observe a vortex lattice does not contradict the spontaneous vortex state scenario.

Finally, it is of interest to compare what a domain wall should look like in the normal vs the spontaneous flux states. The solid line in Fig. 12 is the numerical integration of Eq. (12) over a square SQUID with side 1 μm, at a height of 0.4 μm, for a magnetization $\mathbf{M} = M\text{sgn}(x)$, with $4\pi M = 50$ G. The

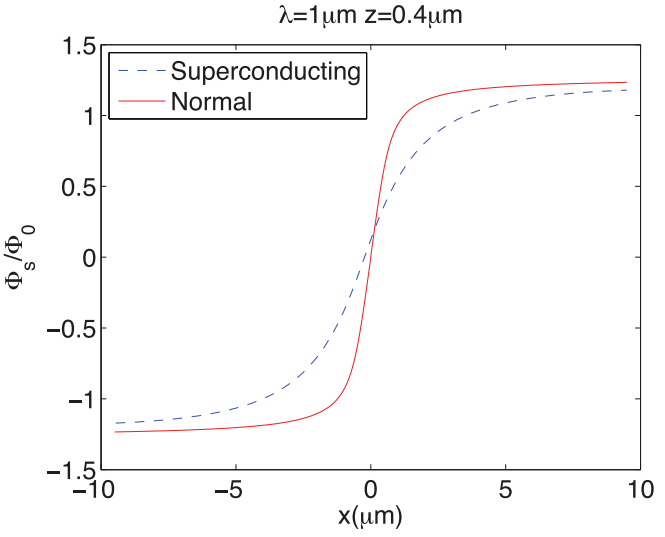

FIG. 12. (Color online) Calculated flux cross section along x for a magnetic superconductor with magnetization $\mathbf{M} = M\text{sgn}(x)\hat{z}$ in the normal state (solid line) and the spontaneous vortex state (dashed line) with the penetration depth $\lambda = 1$ μm, a height $z = 0.4$ μm, a square pickup area of side $s = 1$ μm, with $4\pi M = 50$ G, with the vortex density in the superconducting state chosen to produce an average field $\langle B_z \rangle = 25$ G.

dashed line is for the spontaneous vortex state with a triangular lattice with a vortex density chosen to give an average field of ± 25 G, with the signs of the vortices negative for $x < 0$ and positive for $x > 0$. It is not clear how the vortices would arrange themselves in the vicinity of a domain boundary, but the simulations suggest that the magnetic signature of the domain boundary may be smeared over a length scale set by the penetration depth in the superconducting state. We did not have the spatial resolution to test for this effect in UCoGe.

V. CONCLUSION

We have reported measurements of the ferromagnetic domain structure in superconducting UCoGe by scanning SQUID microscopy. We find a typical domain size of 10 μm in the virgin state and have shown strong evidence for UCoGe to be a perfect Ising magnet with its magnetic moments along the c axis. Diamagnetic screening on the local scale is evidenced by the change in magnetization of the domains when the magnetic field is applied in the superconducting state. When warming the sample under applied field from the superconducting to the normal state domains break up into smaller domains. The Meissner signal could not be detected. The spontaneous vortex phase, $H_{c1} < M$, is consistent with the small change of the domain structure and arrangement upon entering the superconducting phase as is shown by our modeling of the magnetic field at a domain wall of a ferromagnetic superconductor in the normal and the superconducting state. By numerical simulation we explain why the scanning SQUID microscope could not resolve the vortices: the contrast in magnetic field between the vortex center and the inter vortex space decreases exponentially if the probe size is of the order of the intervortex spacing and the penetration depth. In order to visualize vortices in UCoGe the probe used has to be smaller than the intervortex distance, has to be scanned closer to the surface than the intervortex distance and be operated in the self-field of the superconducting ferromagnet. With a typical probe size of less than 500 nm and all other conditions fulfilled vortices will be resolved in the ferromagnetic superconductor UCoGe.

ACKNOWLEDGMENTS

The authors thank T. Crozes for the expert fabrication of the μ-SQUID devices. J.K. was partially supported by the Nanoscience Foundation in Grenoble within the project Chair of Excellence "SuperNanoCharac," and by the NSF NSEC Grant PHY-0425897. This work has also been supported by the French ANR grant SINUS No. ANR- 51609-BLAN-0146.

[1] P. W. Anderson and H. Suhl, Phys. Rev. **116**, 898 (1959).
[2] T. Jarlborg, A. J. Freeman, and T. J. Watson-Yang, Phys. Rev. Lett. **39**, 1032 (1977).
[3] S. Sinha, G. Crabtree, D. Hinks, and H. Mook, *16th International Conference on Low Temperature Physics* [Physica B+C **109-110**, 1693 (1982)], http://www.sciencedirect.com/science/article/pii/0378436382905320.
[4] Ø. Fischer, in *Ferromagnetic Materials*, edited by K. H. J. Buschow and E. P. Wohlfarth, Vol. 5 (Elsevier Science, Amsterdam, 1990), p. 466.
[5] S. S. Saxena, P. Agarwal, K. Ahilan, F. M. Grosche, R. K. W. Haselwimmer, M. J. Steiner, E. Pugh, I. R. Walker, S. R. Julian, and P. Monthoux, Nature (London) **406**, 587 (2000).
[6] T. Akazawa, H. Hidaka, T. Fujiwara, T. C. Kobayashi, E. Yamamoto, Y. Haga, R. Settai, and Y. Onuki, J. Phys.: Condens. Matter **16**, L29 (2004).
[7] D. Aoki, A. Huxley, E. Ressouche, D. Braithwaite, J. Flouquet, J. P. Brison, E. Lhotel, and C. Paulsen, Nature (London) **413**, 613 (2001).
[8] N. T. Huy, A. Gasparini, D. E. de Nijs, Y. Huang, J. C. P. Klaasse, T. Gortenmulder, A. de Visser, A. Hamann, T. Goerlach, and H. v Loehneysen, Phys. Rev. Lett. **99**, 067006 (2007).
[9] N. T. Huy, D. E. de Nijs, Y. K. Huang, and A. de Visser, Phys. Rev. Lett. **100**, 077002 (2008).
[10] A. de Visser, N. T. Huy, A. Gasparini, D. E. de Nijs, D. Andreica, C. Baines, and A. Amato, Phys. Rev. Lett. **102**, 167003 (2009).
[11] A. Gasparini, Y. K. Huang, J. Hartbaum, H. v Loehneysen, and A. de Visser, Phys. Rev. B **82**, 052502 (2010).
[12] T. Ohta, T. Hattori, K. Ishida, Y. Nakai, E. Osaki, K. Deguchi, N. K. Sato, and I. Satoh, J. Phys. Soc. Jpn. **79**, 023707 (2010).
[13] D. Aoki, T. D. Matsuda, V. Taufour, E. Hassinger, G. Knebel, and J. Flouquet, J. Phys. Soc. Jpn. **78**, 113709 (2009).
[14] E. Slooten, T. Naka, A. Gasparini, Y. K. Huang, and A. de Visser, Phys. Rev. Lett. **103**, 097003 (2009).
[15] T. Hattori, Y. Ihara, Y. Nakai, K. Ishida, Y. Tada, S. Fujimoto, N. Kawakami, E. Osaki, K. Deguchi, N. K. Sato *et al.*, Phys. Rev. Lett. **108**, 066403 (2012).
[16] C. Paulsen, D. J. Hykel, K. Hasselbach, and D. Aoki, Phys. Rev. Lett. **109**, 237001 (2012).
[17] M. Faure and A. I. Buzdin, Phys. Rev. Lett. **94**, 187202 (2005).
[18] C. Veauvy and K. Hasselbach, Rev. Sci. Instrum. **73**, 3825 (2002).
[19] D. J. Hykel, Z. S. Wang, P. Castellazzi, T. Crozes, G. Shaw, K. Schuster, and K. Hasselbach, J. Low Temp. Phys. **175**, 861 (2014).
[20] W. Knafo, T. D. Matsuda, D. Aoki, F. Hardy, G. W. Scheerer, G. Ballon, M. Nardone, A. Zitouni, C. Meingast, and J. Flouquet, Phys. Rev. B **86**, 184416 (2012).
[21] S. Chikazumi, *Physics of Magnetism* (John Wiley & Sons, New York, 1964).
[22] D. Aoki, I. Sheikin, T. D. Matsuda, V. Taufour, G. Knebel, and J. Flouquet, J. Phys. Soc. Jpn. **80**, 013705 (2011).
[23] J. Vejpravova-Poltierova, J. Pospisil, J. Prokleska, K. Prokes, A. Stunault, and V. Sechovsky, Phys. Rev. B **82**, 180517 (2010).
[24] H. Bluhm, Phys. Rev. B **76**, 144507 (2007).
[25] M. Tachiki, H. Matsumoto, T. Koyama, and H. Umezawa, Solid State Commun. **34**, 19 (1980).
[26] J. Pearl, J. Appl. Phys. **37**, 4139 (1966).
[27] M. Tinkham, *Introduction to Superconductivity*, 1st ed. (McGraw-Hill, New York, 1975).
[28] N. T. Huy, Ph.D. thesis, van der Waals–Zeeman Instituut, Universiteit van Amsterdam, 2008.